XMOD2 - An improved geophysical model function to retrieve sea surface wind fields from Cosmo-SkyMed X-band data

Francesco Nirchio[1]*and Sara Venafra[2]

[1]Geodesy Space Centre, Agenzia Spaziale Italiana, 75100, Matera, Italy
[2]Politecnico di Bari, Via Orabona 4, 70125, Bari, Italy
*Corresponding author, e-mail address: francesco.nirchio@asi.it

Abstract

This paper presents a semi-empirical geophysical model function to retrieve wind fields from SAR data acquired by the Italian satellite constellation COSMO-SkyMed (CSK). The model is suitable for X-band data with vertical VV polarization. A data set of more than 300 CSK images has been used for the model coefficients estimation. QuikSCAT and Global Forecast System analysis data have been used for model development. The validation of the results has been carried out with a new data set of 24 images acquired over three oceanographic buoys. The agreement between the wind model and in situ data is quite satisfactory. We consider the present results adequate for a large variety of applications.
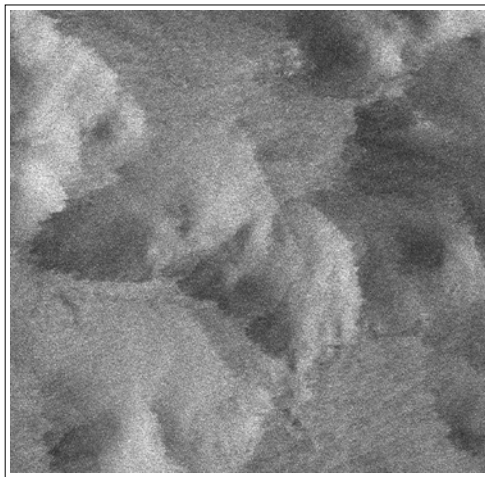**Keywords:** SAR, Wind, X-Band, XMOD2.

Introduction

Observations of wind over the oceans are regularly performed using satellite data that can provide timely global coverage. However, these data do not completely fulfil the spatial requirements of several applications, such as coastal protection or wind farm design [Beaucage et al., 2008]. High-resolution wind data, currently unavailable, could be provided by Synthetic Aperture Radar (SAR) [Vachon and Dobson, 1996; Zecchetto et al., 2008]. The SAR instrument is not specifically designed for this purpose but is of great interest because of the availability of large amounts of data. In addition to the imagery provided by historical missions, such as ERS and ENVISAT, there are now satellite constellations in the X-Band, such as Terrasar-X and Cosmo-SkyMed (CSK), which can be profitably used. The results available for C-Band are not immediately applicable to X-Band, because the geophysical model function (GMF) requires specific parameters in every band. Currently, there are two methods for wind estimation. The first is based on the analysis of the spectral features of SAR imagery [Kerbaol et al., 1996, 1998]; it uses an empirical linear relation to evaluate the wind speed from imagery azimuth cut off frequency. The second approach

retrieves wind intensity from the normalized radar cross section σ_o, which can be expressed as a function of wind intensity, direction and radar incidence angle [Gerling, 1986; Elachi, 1987; Stoffelen and Anderson, 1997; Hersbach, 2002; Shimada et al., 2003]. We have chosen this second method. In this paper, we extend the validity of the geophysical function model XMOD1 [Nirchio and Venafra, 2010] to wind speeds of up to 25 m s^{-1}, because that model was developed and tested for wind speeds in the range of between 2 and 8 m s^{-1}.

The paper is organized as follows: section 2 describes the data set used. In section 3, the calibration procedure and the estimation of the GMF are illustrated. The results are presented in section 4 and the conclusions are reported in section 5.
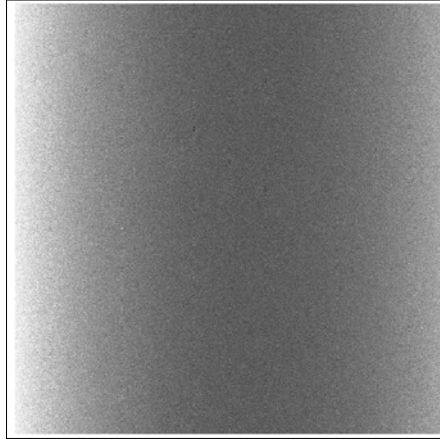
Data set description

XMOD2 has been developed using CSK products; specifically, the VV polarization level 1B Stripmap images. These data have a swath extension wider than 40 km, three equivalent number of looks and ground resolution better than 5 m. The detailed specifications of CSK products are available online at: http://www.cosmo-skymed.it/en/products.htm. For the model definition only, we have selected images of uniform intensity, in order to avoid radar backscatter that could depend not only on wind but also on other features present in the scene [Jackson and Apel, 2004], such as large ships, rain cells and atmospheric fronts (Fig. 1).

Figure 1 - Example of image excluded from the XMOD2 coefficients estimation because of non-uniformity.

We have not taken into account images acquired with an incidence angle greater than 50°, because in that condition, especially at low wind intensities, the backscattering from the ocean surface could be lower than the receiver thermal noise. Figure 2 shows an example of such an occurrence, where the range antenna pattern compensation produces a large backscattering at the image borders.
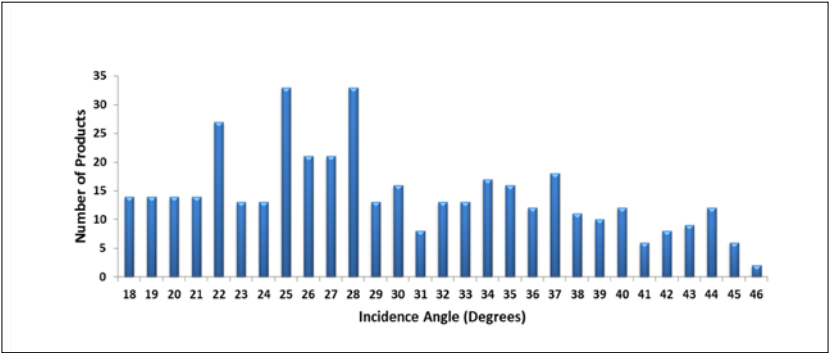
Figure 2 - Example of image in which the backscattering from the ocean surface is lower than the receiver thermal noise.

In collecting data, we have tried to cover uniformly wind intensities up to 25 m s⁻¹. Unfortunately, some ranges are poorly populated, especially the higher regimes. Most of the images have been acquired over the Atlantic Ocean, far from the central African coasts, to exclude the influence of topography and to obtain a wind field that is as uniform as possible. The winds in this area rarely have intensity greater than 14 m s⁻¹; consequently, we have selected some areas at higher latitudes where the winds are stronger. One of these areas is located between Iceland and the British Isles, the second is off the coast of Alaska and the final one is in the Atlantic Ocean off the Canadian coast, as displayed in Figure 3. For the model tuning, we acquired 303 images: 121 of these were off the African coast and 124 at higher latitudes, specifically: 11 images off the eastern Canadian coast, 10 images in the Pacific Ocean off the Alaskan coast and 103 images in the Arctic ocean off the coast of Iceland.
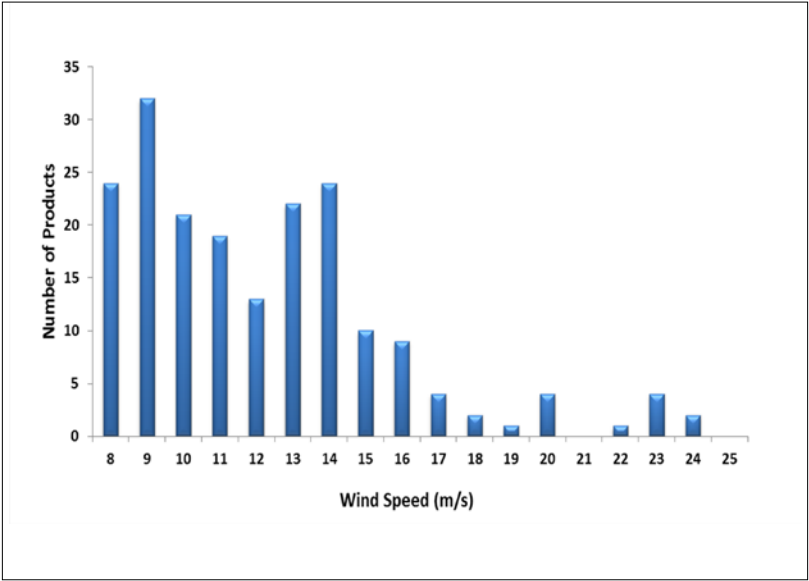

Figure 3 - Ovals are the areas where SAR data have been acquired for XMOD2 development. Stars represent buoys used for validation.
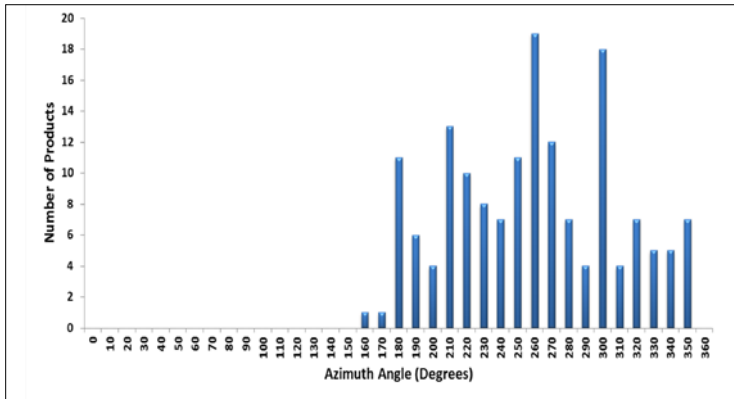
After visual inspection, 53 scenes were rejected because they were deemed unsuitable. Figure 4 shows the number of images covering any incidence angle. In Figure 5, the number of images acquired at different wind conditions is reported and in Figure 6, the distribution of images per wind direction is depicted. The latter is not uniform and this aspect should be improved in the future. In contrast, data used for the model validation have more uniform distribution of wind direction.

Figure 4 - Number of images at different incidence angles for wind speed greater than 8 m/s.

Figure 5 - Number of images acquired off the coasts of Alaska, Canada and Iceland for different wind speeds.

Figure 6 - Number of images acquired per different azimuth angles.

For the estimation of the model coefficients we used two kinds of data: those provided by QuikSCAT, NASA's Scatterometer, operating from 1999 until November 2009; the nominal end of its mission [NASA, 2006] and the Global Forecast System (GFS) analysis data, made available by the National Oceanic and Atmospheric Administration (NOAA). The QuikSCAT wind vector fields, measured at a height of 10 meters over the ocean surface, have spatial resolution of 25 kilometers, wind speed root mean square (RMS) accuracy of 2 m s^{-1} and direction RMS of 20°. The GFS products, both predictions and analysis, were made available by the National Centers for Environmental Prediction (NCEP); they are provided on a grid space of about 50 km at six-hourly intervals. Typically, the Numerical Prediction Model has wind speed RMS error accuracy higher than 2 m s^{-1} and wind direction RMS error of 50°. [Cox et al., 1998; Hou, 2002]. These data can be found at the following site: www.nco.ncep.noaa.gov/pmb/products/gfs/.

XMOD2 validation has been conducted using the data of three buoys owned and maintained by the US National Data Buoy Center (NDBC); specifically, Station 41046 located at 23.838°N 68.333°W (east Bahamas), Station 41044 located at 21.639°N 58.614°W (St. Martin) and Station 51101 located at 24.321°N 162.058°W (Hawaii). The first two are equipped with a 6-metre NOMAD buoy with ARES 4.4 payload; the third is a 3-metre buoy with AMPS payload. They provide data every hour. The wind speed accuracy is +/- 1.0 m s^{-1} or 10%. The wind direction has an accuracy of +/- 10°. Data are available at the following site: http://www.ndbc.noaa.gov. The CSK images acquired over the buoys number 25 in total: 10 for the east Bahamas buoy, 10 for the Hawaiian buoy and 5 for that of St. Martin.

Geophysical Model Function estimation
The strong relation of sea radar backscattering from wind intensity and direction is a well-proven result [Jackson and Apel, 2004]. Bragg scattering has been identified as the main scattering mechanism for incidence angles larger than 20°. It describes the interactions between the centimetre radar wavelengths generally used and the ocean surface short gravity waves and surface-tension waves. The Bragg resonant wavelength depends on the incidence angle; it is larger at steep incidence angles and decreases as the incidence angle increases. Because the ocean wave power spectrum falls off sharply at short wavelengths, the radar

return decreases accordingly. Another parameter playing an essential role in the process is the horizontal angle between the radar look direction and the upwind direction. The maximum signal is received when the radar points towards the upwind direction and it is a minimum when the wind blows perpendicularly to the look angle. The backscattering behaviour is reasonably described by the following mathematical model, which we have adopted for XMOD2 and is similar to the one used for the L, C and Ku bands. Its expression is:

$$\sigma_0 = B_0 \left\{ 1 + B_1 \cos(\phi - \phi_w) + B_2 \cos\left[2(\phi - \phi_w)\right] \right\} \quad [1]$$

where σ_o is the Radar Cross Section (RCS) and ϕ and ϕ_w are the radar ground range direction and upwind direction, respectively. B_0, B_1 and B_2 have the following expressions:

$$B_0 = 10^\beta U^\gamma \quad [2]$$

$$\beta = C(1) + C(2)\theta + C(3)\theta^2 \quad [3]$$

$$\gamma = C(4) + C(5)\theta + C(6)\theta^2 \quad [4]$$

$$B_1 = C(7) + C(8)\theta + C(9)\theta^2 + \left[C(10) + C(11)\theta + C(12)\theta^2\right]U \quad [5]$$

$$B_2 = C(13) + C(14)\theta + C(15)\theta^2 + \left[C(16) + C(17)\theta + C(18)\theta^2\right]U \quad [6]$$

U is the wind intensity in metres per second at a height of 10 metres above sea level, θ is the radar incidence angle in degrees and C(1)-C(18) are 18 coefficients.

First, the radar cross section σ_o was computed because the CSK images are provided in digital number (DN). RCS, the ratio of the backscatter density to the power density that is intercepted by the target, is obtained by compensating for the range spreading loss, the antenna pattern gain and the incidence angle variations of the received signal, as described in [Inversi, 2009]. The expression applied to obtain the σ_o of the area corresponding to image position (i,j), is the following:

$$\sigma_0(i,j) = \frac{img(i,j)^2 \, R_{Ref}^{2R_{exp}} \sin(\alpha_{ref})}{F^2 K} \quad [7]$$

where: R_{Ref} is the calibration reference slant range, R_{exp} is the reference slant range exponent,

α_{ref} is the calibration reference angle, F is the scaling factor, K is the calibration constant and img(i, j) is the CSK image element at the i-th row and j-th column. The above parameters are all reported in the HDF5 image annotations. Some corrections have already been applied during the SAR image production and do not need to be reapplied for the calibration. For this reason, it is necessary to check the calibration flags recorded on each data annotation. In particular, if the range spreading loss compensation geometry parameter is equal to

'None', then the factor $R_{Ref}^{2R_{exp}}$ should be omitted in expression [7]. If the incidence angle compensation geometry parameter is 'None', then the factor $\sin(\alpha_{ref})$ should also be omitted. The calibration constant K should be omitted if the calibration flag parameter is not 1.

The average backscatter intensity σ_o in expression [1] has been computed on 400×400 pixel sub-images. QuikSCAT and GFS estimates of wind speed at each SAR sub-image location were obtained through linear data interpolation. The elapsed time between the QuikSCAT and CSK acquisitions is generally less than one hour. GFS data before and after the CSK acquisition are interpolated over time.

Because XMOD1 [Nirchio and Venafra, 2010] had significant errors for wind intensities greater than 8 m s^{-1}, most likely because of the limited number of images used and owing to a large change in the GMF function slope, we have assumed a similar expression for XMOD2 but have evaluated the model parameters in two adjacent ranges of wind intensities. This solution is inelegant but does have the practical advantage of extending the validity of the previous model. Additionally, CMOD4 has a parameter that is wind intensity dependent.

In deriving the 18 C coefficients, we have proceeded in the following way. First, using the generalised reduced gradient method, we have estimated coefficients B_0, B_1 and B_2 from equation [1] in all those (U,θ) points with at least three available images, in order to have three independent σ_o values. Subsequently, using equation [8] in place of equation [2], we have estimated β and γ for different values of θ.

$$\text{Log}_{10}\, B_0\left(U,\theta\right) = \beta\left(\theta\right) + \gamma\left(\theta\right)\text{Log}_{10}\, U \quad [8]$$

Then, we have obtained coefficients C(1)-C(3), and C(4)-C(6) from equations [3] and [4], respectively with a second order polynomial fitting. Similarly, we have estimated B_1 and B_2 at the same (U,α) points as used for B_0 and we have transformed equations [5] and [6], respectively in the following:

$$B_1\left(U,\theta\right) = D\left(\theta\right) + E\left(\theta\right)U \quad [9]$$

$$B_2\left(U,\theta\right) = F\left(\theta\right) + G\left(\theta\right)U \quad [10]$$

We have evaluated D, E, F and G in the same manner as we have done for β and γ and finally, we have derived coefficients C(7)-C(18) with a second order polynomial fit of the following equations:

$$D = C(7) + C(8)\theta + C(9)\theta^2 \quad [11]$$

$$E = C(10) + C(11)\theta + C(12)\theta^2 \quad [12]$$

$$F = C(13) + C(14)\theta + C(15)\theta^2 \quad [13]$$

$$G = C(16) + C(17)\theta + C(18)\theta^2 \quad [14]$$

We have chosen to derive the 18 C coefficients in successive steps, as described above, instead of using a single global minimisation procedure, because in this way we have easily identified and eliminated the outliers, obtaining a quick convergence of the minimisation method.

In Tables 1 and 2, the estimated values for the 18 C coefficients are reported; specifically, those of Table 1 must be used for wind intensity in the range 2-7 m s^{-1}, whereas those of Table 2 must be used in the range 7-25 m s^{-1}.

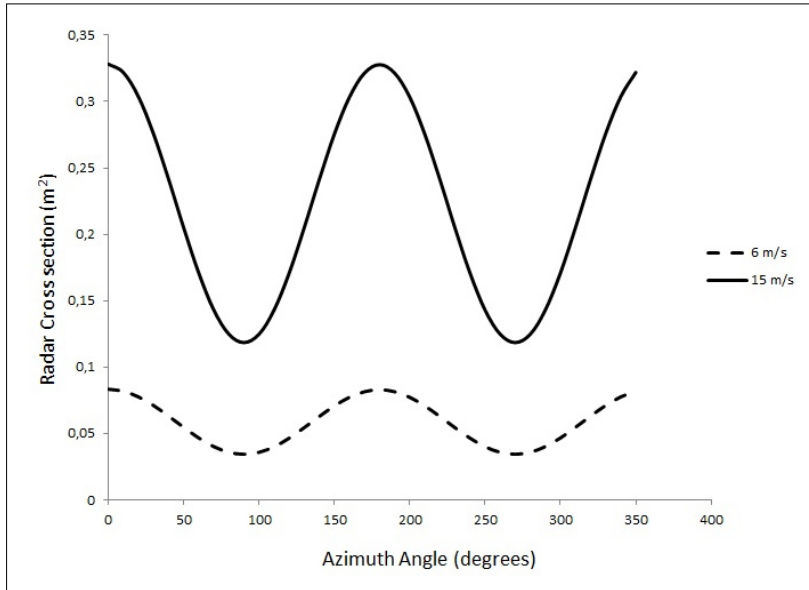**Table 1 - XMOD2 coefficients for wind intensity in the range 2-7 m s^{-1}.**

Parameter	Coefficients	Value	Parameter	Coefficients	Value
β	C(1)	6.657480		C(10)	0.051664
	C(2)	-0.527524		C(11)	-0.002735
	C(3)	0.007124		C(12)	0.000037
γ	C(4)	-4.650782	B$_2$	C(13)	-1.334011
	C(5)	0.402273		C(14)	0.098156
	C(6)	-0.006065		C(15)	-0.001013
B$_1$	C(7)	-0.258321		C(16)	0.316948
	C(8)	0.013675		C(17)	-0.020622
	C(9)	-0.000186		C(18)	0.000283

Table 2 - XMOD2 coefficients for wind intensity in the range 7-25 m s^{-1}.

Parameter	Coefficient	Value	Parameter	Coefficient	Value
β	C(1)	3.152255		C(10)	0.0019511
	C(2)	-0.2694191		C(11)	-0.0001425
	C(3)	0.0029979		C(12)	0.000002
γ	C(4)	-0.450287	B$_2$	C(13)	2.0670443
	C(5)	0.0928452		C(14)	-0.1309205
	C(6)	-0.001101		C(15)	0.0023609
B$_1$	C(7)	-0.0228304		C(16)	-0.1698661
	C(8)	0.0016691		C(17)	0.0124482
	C(9)	-0.000023		C(18)	-0.000211

In Figure 7, some GMF Radar Cross Sections are reported as a function of the azimuth angle between the incidence plane and the wind vector.

Figure 7 - Azimuthal variation of the XMOD2 Radar Cross Section. The incidence angle in both cases is 30°.
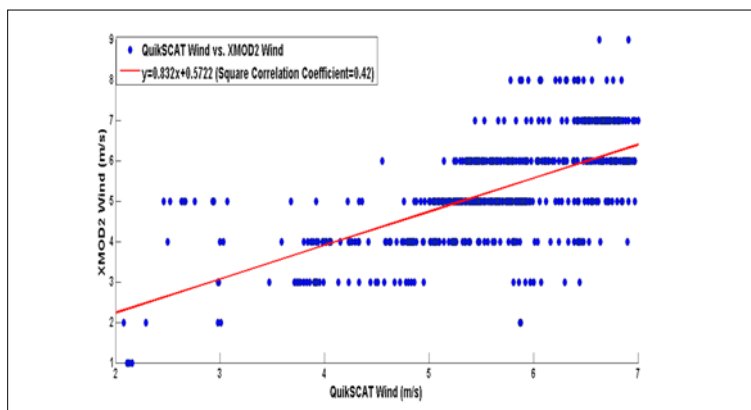
Results

The retrieving wind procedure consists of finding the wind intensity U, which minimizes the following F(U) function:
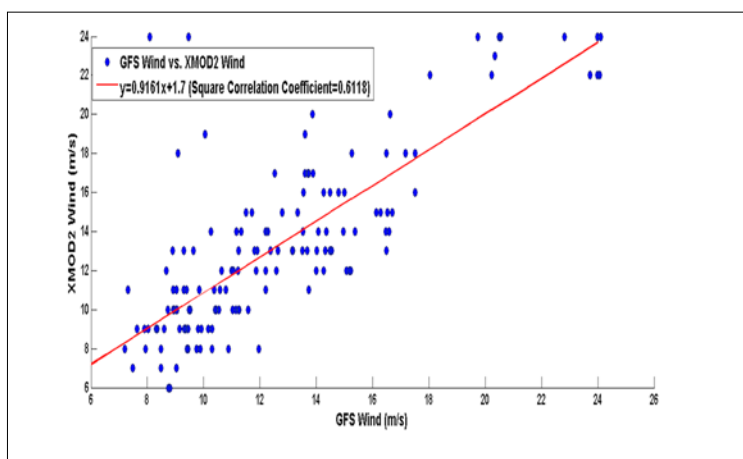
$$F(U) = \left[M\left(U, \phi\right) - \sigma_0 \right]^2 \quad [15]$$

where: σ_o is the radar cross section measured on the SAR imagery, M(U, ϕ) is that predicted by XMOD2 and ϕ is the angle between the look angle and the wind direction. In this study, we relied on wind direction information gathered from external data, i.e., QuikSCAT, GFS and the buoys.

For a first model evaluation, we have computed the wind intensity on the data set used to derive the C coefficients. On 53 SAR images with winds up to 7 m s^{-1} we have compared XMOD2 and QuikSCAT wind speeds. For each image, we have measured wind on 12 regularly spaced 1 km square sub-images. QuikSCAT wind estimates collocated with SAR measurements were obtained through an interpolation of the closest QuikSCAT data. We have excluded 10 measurements that owing to local phenomena were significantly higher than other data. Figure 8 depicts the result of this comparison. The RMS difference between XMOD2 and QuikSCAT wind speeds is 0.8 m s^{-1}.

Figure 8 - Scatterplot of QuickSCAT wind speed versus XMOD2 wind speed for speeds lower than 7 m s^{-1} . 640 measurements on 53 images.
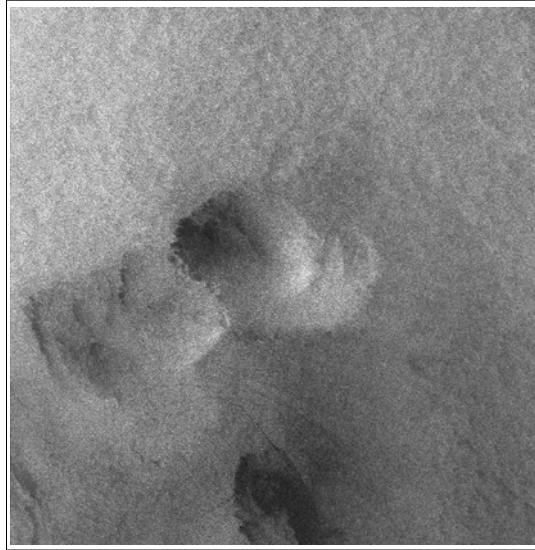
The analysis of winds in the range 7-25 m s^{-1} has been conducted on a data set of 121 images, the majority of which were acquired after November 2009, when only GFS data were available. In this case, we have considered 12 measurements per scene. We have interpolated over time the GFS data acquired before and after the CSK overpass and then interpolated them in space in order to have collocated SAR and GFS wind estimations. In this case, we found an RMS difference of 2.0 m s^{-1}.

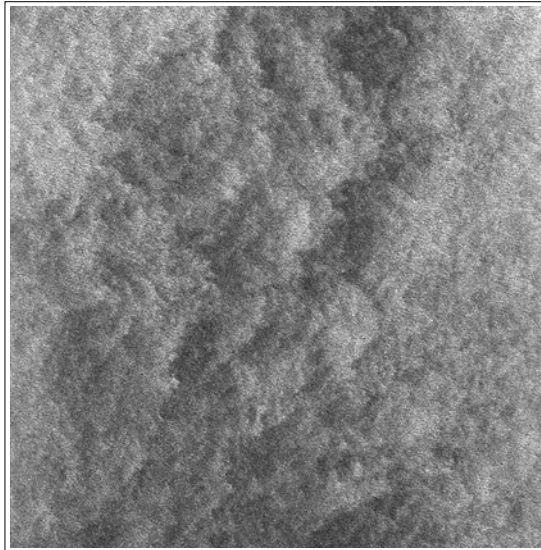**Figure 9 - Scatter plot of GFS wind speed versus XMOD2 wind speed for speeds in the range 7-25 m s^{-1}.**

Concerning the validation, we have used a data set of 25 images acquired between 31/01/2013 and 16/02/2013 and real-time buoy data. According to NDBC, these real-time data have undergone gross error checking only. For the wind retrieval, we used the wind direction provided by the buoys. We have discarded one image on the grounds of bad quality. The images

analyzed are far from uniform. They present a variety of local phenomena, such as rain cells, atmospheric fronts, convective cells and swells. Two examples are provided in Figures 10 and 11. We have computed the wind speed on a 400 × 400 m square sub-image, exactly collocated with the buoys. The maximum time lag between the SAR and buoy data is one hour.
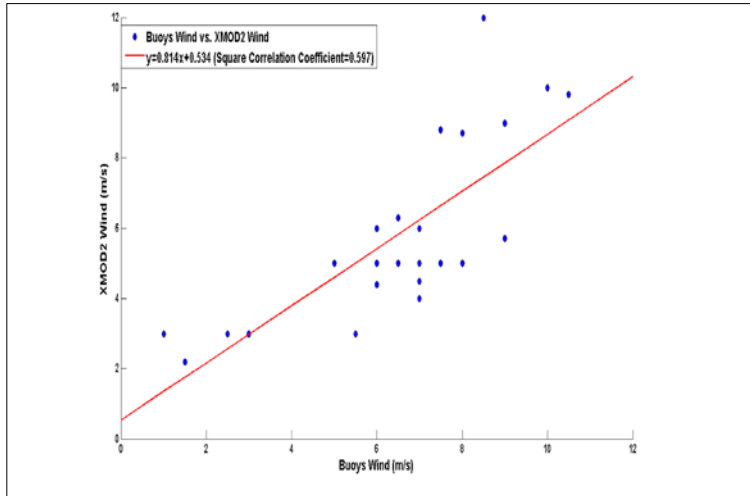

Figure 10 - Image acquired by CSM4 over buoy station 41046 (East Bahamas) on 7/02/2013.

Figure 11 - Image acquired by CSM4 over buoy station 41046 (East Bahamas) on 12/02/2013.

The result of XMOD2 and the buoy wind comparison is depicted in Figure 12. The RMS difference is 1.3 m s^{-1}. We explain some of the variability of the measurements by local phenomena. The XMOD2 and buoy comparison is in line with the results obtained by other similar campaigns.

Figure 12 - Scatterplot of XMOD2 wind speed versus buoy wind speed.

Conclusions

We have developed a semi-empirical model to estimate the wind intensity from X-Band SAR data. The model, derived using Cosmo-SkyMed data, has been tested on an extended range of wind intensities between 2 and 25 m s^{-1}. The results are in good agreement with ground truth data. According to the present outcomes, XMOD2 could be used operationally for several applications, which require a high-resolution in situ wind field. We expect further improvements on the model's performance when a more complete imagery data set becomes available and the wind direction is estimated directly from the SAR data.

Acknowledgements

References

Beaucage P., Bernier M., Lafrance G., Choisnard J. (2008) - *Regional mapping of the offshore wind energy assessment: Towards a significant contribution from space-borne synthetic aperture radars*. IEEE Journal of Selected Topics in Applied Earth Observations and Remote Sensing, 1: 48-56. doi: http://dx.doi.org/10.1109/JSTARS.2008.2001760.

Cox R., Bauer B.L., Smith T. (1998) - *A mesoscale model intercomparison*. Bulletin of the American Meteorology Society, 79: 265-283. doi: http://dx.doi.org/10.1175/1520-0477(1998)079<0265:AMMI>2.0.CO;2.

Elachi C. (1987) - *Spaceborne radar remote sensing: applications and techniques*. Elachi C. Eds., IEEE Press, New York, pp. 202-204.

Gerling T.W. (1986) - Structure *of the surface wind field from the Seasat SAR*. Journal of Geophysical Research, 91 (C2): 2308-2320. doi: http://dx.doi.org/10.1029/JC091iC02p02308.

Hersbach H. (2002) - *An Improved Geophysical Model Function for ERS C-Band Scatterometry*. Available online at: http://earth.esa.int/pub/SCATTEROMETER/ecmwf_rep/cmod5.pdf.

Hou D. (2002) - *Evaluation of high resolution NWP Model Output of Near-Surface Variables*. 12th PSU/NCAR Mesoscale Model Users Workshop, Boulder.

Inversi P. (2009) - *Cosmo/SkyMed image calibration*. Available online at: www.e-geos.it/products/pdf/COSMO-SkyMed-Image_Calibration.pdf.

Jackson C.R., Apel J.R. (2004) - *Synthetic Aperture Radar Marine User's Manual*. Washinton, DC, U.S. Department of Commerce, p. 464. Available on line at: http://www.sarusersmanual.com.

Kerbaol V., Chapron B., Elfouhaily T., Garello R. (1996) - *Fetch and Wind Dependence of SAR Azimuth Cutoff and Higher Order Statistics in a Mistral Wind Case*. International Geoscience and Remote Sensing Symposium IGARSS'96, 21-26 May 1996, Lincoln, Nebraska, USA.

Kerbaol V., Chapron B., Vachon P.W. (1998) - *Analysis of ERS-1/2 SAR Wave Mode Imagettes*. Journal of Geophysical. Research., 103 (C4): 7833-7846. doi: http://dx.doi.org/10.1029/97JC01579.

NASA *Quick Scatterometer QuikSCAT Science Data Product User's Manual Version 3*. September 2006 D-18053. Available on line at: ftp://podaac.jpl.nasa.gov/allData/quikscat/L2B/v2/docs/QSUG_v3.pdf.

Nirchio F., Venafra, S. (2010) - *Preliminary model for wind estimation from Cosmo/SkyMed X band SAR data*. Proceedings of International Geoscience and Remote Sensing Symposium IGARSS 2010, 25-30 July 2010, Honolulu, Hawaii, USA, pp. 3462-3465. doi: http://dx.doi.org/10.1109/IGARSS.2010.5650437.

Shimada T., Kawamura H., Shimada M. (2003) - *An L-band geophysical model function for SAR wind retrieval using JERS-1 SAR*. IEEE Transaction on Geoscience and Remote Sensing, 41: 518-531. doi: http://dx.doi.org/10.1109/TGRS.2003.808836.

Stoffelen A., Anderson D. (1997) - *Scatterometer Data Interpretation: Measurement Space and inversion*. Journal of Atmospheric and Oceanic Technology, 14 (6): 1298-1313. doi: http://dx.doi.org/10.1175/1520-0426(1997)014<1298:SDIMSA>2.0.CO;2.

Vachon P.W., Dobson F.W. (1996) - *Validation of wind vector retrieval from ERS-1 SAR images over the ocean*. The Global Atmosphere and Ocean System, 5: 177-187.

Zecchetto S., Nirchio F., Di Tomaso S., De Biasio F. (2008) - *Similarities and differences of SAR derived wind fields using two different methods: the local gradient and the continuous wavelet transform methods*. Proceedings of 2nd International Workshop on Advances in SAR Oceanography from ENVISAT and ERS missions, 21-25 January 2008, Frascati, Italy.